DOI: 10.31276/VJSTE.65(3).50-58

Synthesising nanocomposite Co_2SnO_4@rGO for peroximonosulphate activation in a hybrid ozonation system to effectively degrade cefalexin from wastewater

Van Long Nguyen, Minh Thanh Le, Lan Huong Nguyen*

Ho Chi Minh City University of Industry and Trade (HUIT), 40 Le Trong Tan Street, Tay Thanh Ward, Tan Phu District, Ho Chi Minh City, Vietnam

Received 16 September 2022; revised 13 November 2022; accepted 20 November 2022

Abstract:

This study successfully developed Co_2SnO_4@rGO nanocomposites at various composite ratios of Co_2SnO_4 and rGO using the sol-gel method. These nanocomposites were then used as heterogeneous catalysts to activate PMS in the heterogeneous catalytic oxidation of Co_2SnO_4@rGO/PMS as well as the hybrid ozonation system O_3/Co_2SnO_4@rGO/PMS to degrade cefalexin (CFX). The physical-chemical characteristics of the fabricated catalysts were evaluated through nitrogen adsorption-deadsorption, SEM images, EDS mapping, and XRD. The catalytic activity of the nanocomposite was investigated in a degradation reaction of CFX from an aqueous solution. Besides this, CFX degradation kinetics were determined by fitting experimental data with a first-order model. The results showed that at the composite ratio of 2-Co_2SnO_4 and 1-rGO for CFX degradation had the highest efficiency reaching 95.07 and 99.07% for Co_2SnO_4@ rGO/PMS and O_3/Co_2SnO_4@rGO/PMS systems, respectively. The degradation of CFX in the O_3/Co_2SnO_4@rGO/ PMS system was higher than that of Co_2SnO_4@rGO/PMS. The results were due to a remarkable increase in S_{BET} in 2-Co_2SnO_4@1-rGO compared to both Co_2SnO_4 and rGO, facilitating a catalytic reaction occurring on the catalyst's surface. Moreover, the coupling between O_3 and Co_2SnO_4@rGO/PMS generated a synergetic effect leading to the generation of more $^*SO_4^-$ and $^*OH$ radicals, which enhanced the CFX degradation rate in the hybrid ozonation system. These primary findings illustrated that the nanocomposite catalyst 2-Co_2SnO_4@1-rGO was feasible for the activation of PMS in hybrid ozonation to effectively degrade antibiotic residues from wastewater.

Keywords: **cephalexin, Co_2SnO_4@rGO, hybrid ozonation, O_3, PMS, synthesis.**

Classification numbers: **2.2, 5.3**

1. Introduction

Today, a large amount of antibiotic residues are being found in natural water bodies such as ponds, lakes, rivers, and effluent after secondary treatment [1]. The discharge from hospital, domestic, livestock, and pharmaceutical wastewater has increased antibiotic residues in these receiving water bodies [2]. The presence of antibiotics in aquatic environments is becoming a major concern around the world due to increases in bacterial resistance towards pharmaceuticals [1]. Penicillin and cephalosporin, a group of β-lactam antibiotics that can break down the synthesis of bacterial cell walls and prevent bacterial growth, have been the most widely used around the world to treat bacterial infections accounting for 50-70% of all antibiotics used [3]. Such high consumption of antibiotics inevitably leads to their release into receiving water bodies [4]. Among the antibiotics from the cephalosporin family, CFX is a systemic antibiotic that is most commonly used to treat respiratory tract infections, urinary tract infections, and skin and soft tissue infections caused by sensitive bacteria [5, 6]. Besides, CFX possesses a very low biodegradation rate, nearly 10%, with 90% being excreted through urine causing increasing environmental concern of antibiotic resistance [7, 8]. Recent studies have shown that the CFX concentration found in wastewater, surface water, and even sea water ranges from several ng/l to µg/l [9, 10]. The accumulation of CFX in the environment leads to an occurrence of multi-drug resistant pathogens, which have unpredictable impacts on the environment, human health, and other organisms in the ecosystem [11].

Due to the complex chemical structure and antibacterial properties of CFX, conventional wastewater treatments such as physical, chemical, physicochemical, and biological methods are not effective to remove this compound [11, 12]. Meanwhile, advanced oxidation processes using strong oxidant agents such as O_3, H_2O_2, and PMS in combination

*Corresponding author: Email: huongnl@hufi.edu.vn

with heterogeneous catalysts possess some advantages thanks to generation of free radicals like $^{*}SO_4$, $^{*}OH$, $^{*}O_2$, and $^{1}O_2$. These are very strong oxidation radicals that can oxidize near-persistent organic compounds and antibiotic residues with quick rates and without the formation of by-products. Among these AOPs, advanced sulphate radical ($^{*}SO_4^{-}$)-based oxidation processes using heterogeneous catalysts to activate PMS for the generation of OH, $^{*}SO_4^{-}$, and ozonation have been reported effective in the removal of persistent organic compounds. However, using only heterogeneous catalysts/PMS or O_3 to degrade pollutants have several limitations such as high cost, low stability, and slow oxidation rate. Therefore, to remedy these drawbacks, some hybrid ozonation processes have been recently applied such as O_3/PMS to degrade ibuprofen [13]; O_3/MnO_2@rGO/PMS for removal of 4-nitrophenol [14]; and O_3/PMS to treat para-chlorobenzoic acid [15]. The results of these works indicate that all hybrid ozonation systems demonstrate high removal efficiencies of pollutants compared to using oxidation systems alone due to the synergetic effects between O_3, PMS, and catalysts in the same reactor.

Recently, cobalt-based catalysts have been developed, popularly used, and proven to be the most effective in heterogeneous catalytic systems to activate PMS, thereby promoting the production of $*SO_4^{-}$ radicals due to the high activation efficiency of Co on PMS [16]. For example, M. Stoyanova, et al. (2014) [17] applied $CoFe_2O_4$ to activate PMS for the mineralization of acid orange 7 while others have used MFe_2O_4/PMS for the removal of di-n-butyl phthalate (DBP) (with the highest activation efficiency in the order $CoFe_2O_4$ > $CuFe_2O_4$ > $MnFe_2O_4$ > $ZnFe_2O_4$) [18]; $CoMn_2O_4$ - activated PMS for a Fenton-like reaction to degrade organic dyes [19]; and $Fe_{0.8}Co_{2.2}O_4$ to remove bisphenol A [20]. Co_2SnO_4 was also used to activate PMS for the degradation of rhodamine B and pentachlorophenol with complete removal of both rhodamine B and pentachlorophenol in a 10 - min reaction [21]. However, cobalt oxide exhibits a disadvantage due to the leakage of metal Co into the water after catalysis, especially under acidic conditions [22]. Therefore, to prevent leakage of Co, a cobalt oxide catalyst can be composited with other metal oxides [23], magnetic molecules [24], biochar [25, 26], or graphite (GO, rGO) [27]. Indeed, compositing metal oxides with graphite is considered effective for the prevention of the abovementioned catalyst drawbacks. Among such nanocomposites, the transition metal cobalt has been the most effectively and widely used. For instance, a composite catalyst of nano-$CoFe_2O_4$ and graphite ($CoFe_2O_4$@GO) has been synthesised to degrade amoxicillin (AMX) from water [28]. The results showed that possessed good magnetic properties and was quickly separated from the aqueous medium after the reaction. $CoFe_2O_4$@GO also exhibits a rather good catalytic activity in the activation of PMS to produce $^{*}SO_4^{-}$. To be specific, at optimal conditions, 99.27, 83.1, and 61.11% of AMX, COD, and TOC were removed after 60 min of reaction, respectively [28]. $CoFe_2O_4$@GO was also used for the activation of PMS in the degradation of RB5 [29] and RB [30]. A hybrid nanocomposite of reduced graphite oxide rGO and $CoFe_2O_4$ ($CoFe_2O_4$/rGO) for the activation of PMS for phenol degradation has also been performed [31]. Indeed, catalytic testing showed that $CoFe_2O_4$/rGO exhibits much better catalytic activity compared with $CoFe_2O_4$, indicating that rGO plays an important role in the $CoFe_2O_4$/rGO hybrid-nanocomposite for the degradation of phenol. In the $^{*}SO_4^{-}$-based heterogeneous catalytic system for the degradation of on organic pollutants, $CoFe_2O_4$/rGO was synthesised using a surface hydrothermal method to activate PMS to degrade phenol with a high degradation efficiency thanks to its large specific surface and 3D structure that promotes mass transfer and dispersion of the catalytic sites on the surface of the $CoFe_2O_4$/rGO aerogel [32].

However, rapid oxidation rates cannot be achieved if PMS, PMS activated by catalysts, or ozonation are used separately. Therefore, hybrid processes between O_3 and PMS-activated heterogeneous catalysts are advantageous in the decomposition of difficult-to-biodegrade organic matters due to the creation of synergistic effects that accelerate the decomposition rate of organic pollutants and increase the efficiency of PMS use, which then reduces the dose of PMS necessary for decomposition. The addition of O_3 to a heterogeneous catalytic system has been shown to increase the activation of PMS and generate both $^{*}OH$ and $^{*}SO_4^{-}$ free radicals. However, studies of this hybrid technology in the treatment of difficult-to-biodegrade organic compounds are rare, especially in the treatment of antibiotic residues. Therefore, the aim of this study was to fabricate a nanocomposite catalyst based on a composite of Co_2SnO_4 and rGO, which was used to activate PMS in a hybrid ozonation system for the enhanced degradation of CFX from wastewater. To reach this aim, this study focused on investigating the most suitable conditions for the synthesis of Co_2SnO_4@rGO and using Co_2SnO_4@rGO as a heterogeneous catalyst to activate PMS in a hybrid ozonation system for the degradation of CFX from water medium.

2. Materials and methods

2.1. Chemicals and materials

All chemicals including $KMnO_4$, H_2SO_4, H_2O_2 (30%), HCl, $CoCl_2$, $SnCl_4$, ethylene glycol, and NaOH were purchased from Kyamata (Japan). $NaBH_4$ and CFX ($C_{16}H_{17}N_3O_4S$) were obtained from Sigma Aldrich (Germany). Graphite used for the fabrication of rGO was purchased from Merck (Germany). All chemicals were used as received without further purification.

2.2. Preparation of catalyst materials

In this study, the synthesis procedure of the nanocomposite Co_2SnO_4@rGO consisted of two main steps:

(1) Firstly, Co_2SnO_4NPs and GO were synthesised separately according to the method modified from W.S. Hummers and R.E. Offeman (1958) [33].

Synthesis of GO: Graphene oxide was prepared from natural graphite powder and exfoliated by common chemical agents according to the modified Hummers method. In the first step of the procedure, 3 g of graphite was placed into a beaker containing 150 ml of 98% sulfuric acid, which was cooled in an ice bath (3-5ºC) and completely agitated. Next, 10.5 g of $KMnO_4$ was gradually added into the mixture for 20 min with stirring for a further 20 min. The mixture was then cooled to room temperature and stirred for 72 h. Following that, 250 ml distilled water and 5 ml of 30% H_2O_2 were supplemented in the mixture to achieve a yellow solution. The obtained solid was filtered and repeatedly washed with 3% HCl and distilled water. Finally, the obtained graphene oxide was dispersed overnight into distilled water, reduced metal ions, and protons using a dialysis bag and stored in the dark.

Synthesis of Co_2SnO_4NPs: The magnetic Co_2SnO_4NPs were synthesised using the sol-gel method. Firstly, 93 g of citric acid was poured in a beaker containing 100 ml of distilled water and agitated in a magnetic stirrer at 120 rpm under 60ºC for 15 min to obtain a clear liquid. In the next step, a mixture of 0.36 g $CoCl_2.6H_2O$, 0.63 g $SnCl_4.6H_2O$, and 40 ml ethylene glycol was added in the above beaker and heated to 80ºC until the mixture completely dissolved. Then, the mixture was heated up to 130ºC to obtain a gel mixture. The gel mixture was heated up to 150ºC for 12 h until it became a completely dry solid. The solid was baked at 300ºC for 3 h under oxygen conditions. Finally, the obtained solid was then furnaced to 1000ºC for a further 2 h and cooled to room temperature (25±2ºC). The obtained black solid were Co_2SnO_4NPs and were stored in sealed plastic bags to use as a precursor for the synthesis of nanocomposite Co_2SnO_4@rGO.

(2) Synthesising nanocomposite Co_2SnO_4@rGO: The Co_2SnO_4@rGO at various ratios were prepared using Co_2SnO_4 NPs and GO, which were achieved from the abovementioned procedures. At the beginning of the procedure, a certain amount of GO was dispersed in a beaker containing 20 ml deionised water and sonicated for 60 min. Then, a pre-determined amount of Co_2SnO_4 NPs were also dispersed into the beaker and sonicated for a further 30 min. Afterwards, 10 ml of 0.1 M $NaBH_4$ was gradually added to the mixture. The mixture was sonicated for a further 30 min. Finally, the achieved precipitate was separated by filtration or centrifugation and cleaned by deionised water and ethanol several times. The precipitate was then vacuumed at 80ºC for 6 h. The obtained product was the Co_2SnO_4@ rGO nanocomposite at different composite ratios. The products were stored in sealed plastic bags and labelled as 1-Co_2SnO_4@1-rGO; 2-Co_2SnO_4@1-rGO; 3-Co_2SnO_4@1-rGO; 1-Co_2SnO_4@2-rGO; and 1-Co_2SnO_4@3-rGO for use in the following experiments. The synthesis procedure of the Co_2SnO_4@rGO nanocomposite is summarized in Fig. 1.

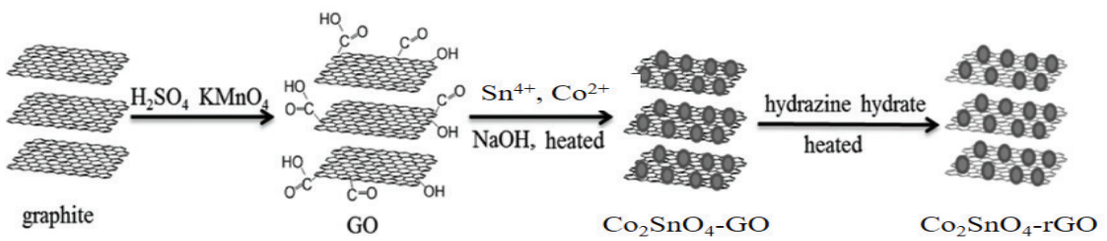

Fig. 1. Schematic description of the synthesis of Co_2SnO_4@rGO nanocomposites.

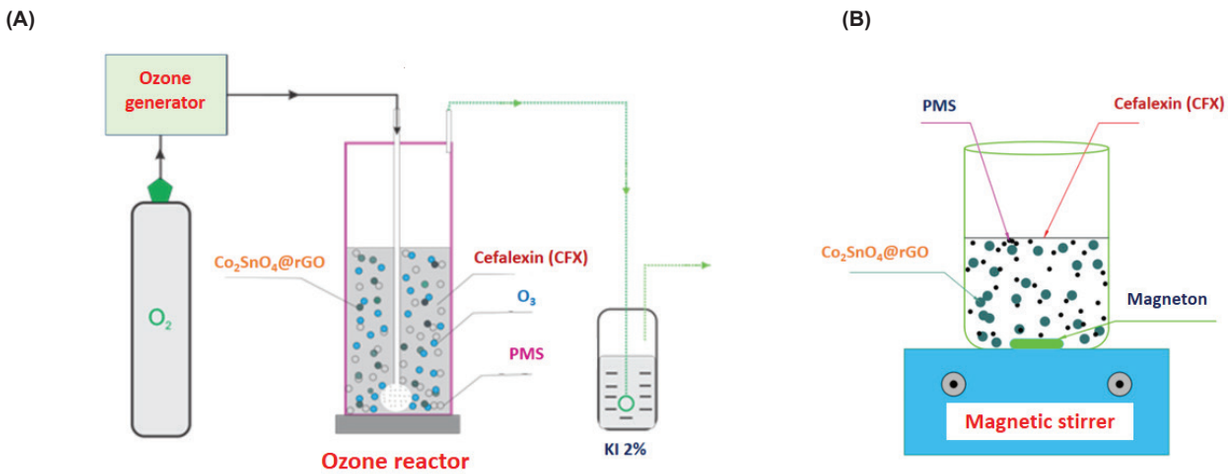

Fig. 2. Scheme of degradation of CFX by O_3/Co_2SnO_4/PMS (A) and Co_2SnO_4/PMS (B).

2.3. Catalytic activity measurement

In this study, CFX was the target pollutant. The CFX degradation experiments were conducted with initial conditions of: CFX concentration of 100 mg/l, pH of 7, catalyst dosage of 0.3 g/l, and PMS dosage of 300 mg/l using Co_2SnO_4@rGO at various composite ratios. All experiments were performed in batch mode. The scheme of CFX degradation by O_3/Co_2SnO_4/PMS and Co_2SnO_4/PMS systems are shown in Fig. 2.

In the O_3/Co_2SnO_4/PMS system, ozone is produced by an ozone generator (NextOzone 20P, Sinh Phu Joint Stock Company, Vietnam). The maximum capacity of O_3 and input O_3 capacity at a flow of 15 ml/min were 5.0 and 3.038 g/h, respectively. The oxygen provided for the O_3 generator was from a pure oxygen container. O_3 is constantly produced and allocated into a tubular borosilicate glass reactor with a height of 450 mm and a diameter of 60 mm through a bubble air stone located at the bottom of the container.

In the Co_2SnO_4/PMS system, the experimental model was set up using a beaker with a volume of 1000 ml containing 500 ml of CFX solution at 100 mg/l and the reaction conditions as abovementioned. The reactor was put on a magnetic stirrer and agitated at 120 rpm.

The reaction kinetics of CFX degradation on the nano-hybrid systems followed a first-order kinetic model (Eq. 1):

$$ln\frac{C_t}{C_o} = -k_d t$$

where C_t is the left concentration of CFX at time t; C_o is the initial concentration of CFX, and k_d is the first-order reaction rate constant. By plotting -ln(C_t/C_o) verse time, k_d and R^2 are determined.

In both reaction systems, the sample was taken out at 40-min intervals to determine the quantity of CFX remaining after reaction.

The CFX removal experiments were triplicated. The results were expressed as average value ±standard deviation.

2.4. Analysis method

The textural characteristic of materials was analysed using N_2 adsorption-desorption isotherms at 77 K (Quantachrome Instruments version 11.0-NOVA). SEM images were applied to observe the morphology of the catalysts using a Hitachi S-4800 (Japan). The EDX data and mapping data were analysed by X-ray energy-dispersive spectroscopy using the JSM-IT200 (InTouchScop). The phase composition and crystal structure of the nanomaterials at various composite ratios were measured by X-ray diffraction with a scanning speed of 1.25°/min at 2θ angles between 20 and 80° using a Bruker D8 device with Cu Kα emission (λ=0.1540 nm).

The degree of CFX degradation was measured using UV-Vis (Shimadzu, model Z2000, Japan) at λ=262 nm. The pH was measured with a pH meter (HANNA, pH HI 2211-02, Romani).

3. Results and discussion

3.1. Characteristics of catalysts

The textural characteristics of the catalysts are presented in Table 1. As can be seen from the data in Table 1, composites of Co_2SnO_4 nanoparticles and rGO led to a remarkable change in the structure of the catalyst. Specifically, at a composite ratio of 2-Co_2SnO_4 and 1-rGO, the S_{BET} of was increased about 17 and 3.9 times compared with Co_2SnO_4 and GO, respectively. Specifically, the S_{BET} of Co_2SnO_4 was 25.43 m^2/g, which agreed with previous work reported by M.B. Ali, et al. (2017) [34]. These results illustrate that the existence of rGO effectively improved the surface property of 2-Co_2SnO_4@1-rGO. The growth of S_{BET} after compositing could be because GO possesses a very large specific surface area in its inherent nature and plays the role of support for Co_2SnO_4. According to IUPAC

Table 1. Nitrogen adsorption-desorption isotherm data of materials.

	Unit	Co_2SnO_4	GO	2-Co_2SnO_4@1-rGO
S_{BET}	m^2/g	25.43	112.9	435.432
V_{pore}	cm^3/g	0.087	0.412	0.383
D_{pore}	nm	0.07	0.94	0.127

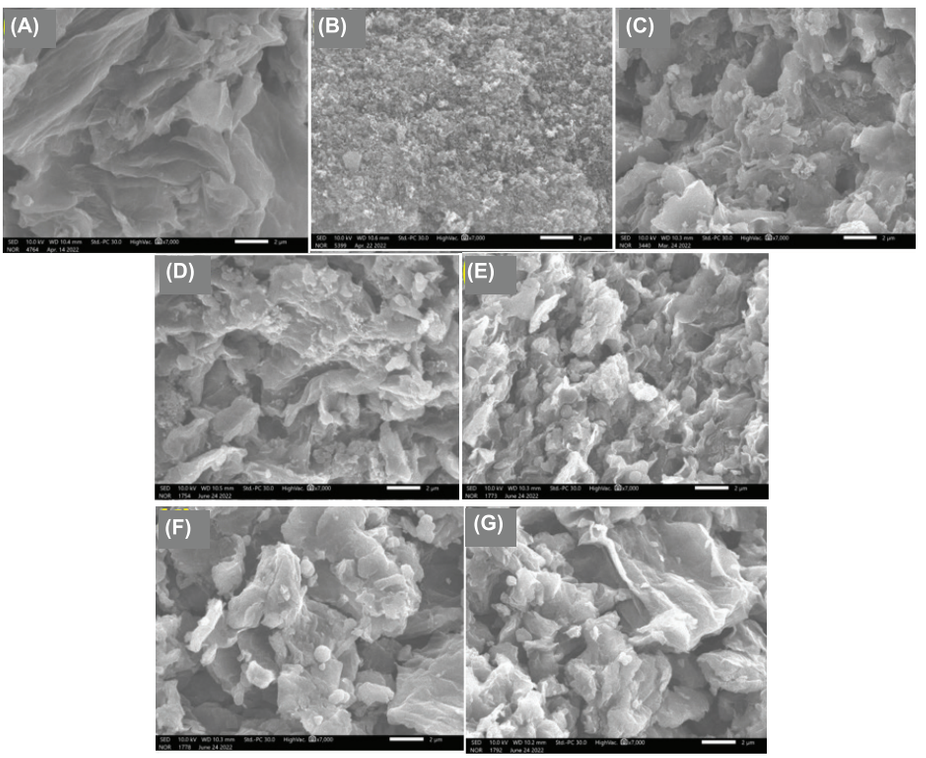

Fig. 3. SEM images of Co_2SnO_4@rGO at various modification ratios. (A) GO, **(B)** Co_2SnO_4, **(C)** 1-Co_2SnO_4@1-rGO, **(D)** 2-Co_2SnO_4@1-rGO, **(E)** 3-Co_2SnO_4@1-rGO, **(F)** 1-Co_2SnO_4@2-rGO, **(G)** 1-Co_2SnO_4@3-rGO.

classification, the 2-Co_2SnO_4@1-rGO nanohybrid had a type-IV isotherm with an H3 hysteresis loop, showing its mesoporous nature. The S_{BET} of 2-Co_2SnO_4@1-rGO was calculated to be 335.432 m^2/g. A similar result was obtained by A.H. Mady, et al. (2019) [27] when compositing γ-MnO_2@$ZnFe_2O_4$ with rGO with an S_{BET} of 376.88 m^2/g. The high surface area provides more adsorption/reaction sites for the activation of PMS during the catalytic reaction, leading to higher catalytic activity.

The morphologies of Co_2SnO_4@rGO at various composite ratios were observed using SEM. The results are demonstrated in Fig. 3. From Fig. 3A, the SEM image of GO showed a regular lamellar structure with drapes of GO. Meanwhile, Fig. 2B displays a typical SEM image of Co_2SnO_4, which indicates particles in an aggregated form with a formation of spherical and cubic nanoparticles. Besides, it is clear that most of the NPs had uniform crystallite size. Figs. 3C-3F, G indicate the morphology of Co_2SnO_4@rGO at various composite ratios. The SEM results showed that Co_2SnO_4@rGO possessed a heterogamous structure with rough surface and Co_2SnO_4 nanoparticles appeared on the surface of nanocomposite. Besides, the transparent silk yarn lamella structure of graphene is more obvious when the GO dosage was increased (Figs. 3E, 3F). Especially, the spherical Co_2SnO_4 particles were more homogeneously loaded on the surface and edges of rGO (Fig. 3D) and the particle size is smaller than those in Fig. 3B, which suggests that agglomeration has been weakened due to the effective fixation and dispersion of rGO on the surface of the Co_2SnO_4 particles. Therefore, it was concluded that the optimum loading ratio of Co_2SnO_4 and rGO was 2:1.

The EDX spectrum of the GO, Co_2SnO_4 NPs, and Co_2SnO_4@rGO at various composite ratios (Fig. 4) essentially show the presence of Co, Sn, C, and O elements indicating good purity of the as-prepared materials. Besides, mapping data also showed a distribution of the constituent elements of Co_2SnO_4@rGO (Fig. 4H). When increasing the composite ratio of Co_2SnO_4, the amounts of Co and Sn elements of Co_2SnO_4@rGO also grew (Figs. 4C-4E). Especially at a composite ratio of 2-Co_2SnO_4 and 1-rGO (Fig. 4D), the amount of Co was the highest. However, when rGO was increased, almost no Co or Sn elements were found in Co_2SnO_4@rGO. The transition metal Co has been proven to effectively activate PMS in catalytic reactions for the degradation of persistent organic compounds. Thus, the Co_2SnO_4@rGO catalyst at a composite ratio of 2-Co_2SnO_4 and 1-rGO was the optimal ratio and used for the rest of this study.

Figure 5 depicts typical XRD patterns of GO, Co_2SnO_4 NPs, and Co_2SnO_4@rGO at various composite ratios synthesised by the sol-gel method. Clearly, the GO pattern has a typical peak at 9.7° corresponding to the (001) crystal plane. However, this characteristic peak was smaller in the Co_2SnO_4@rGO X-ray diffraction and a small diffraction peak appeared at 19°, which suggested that GO was

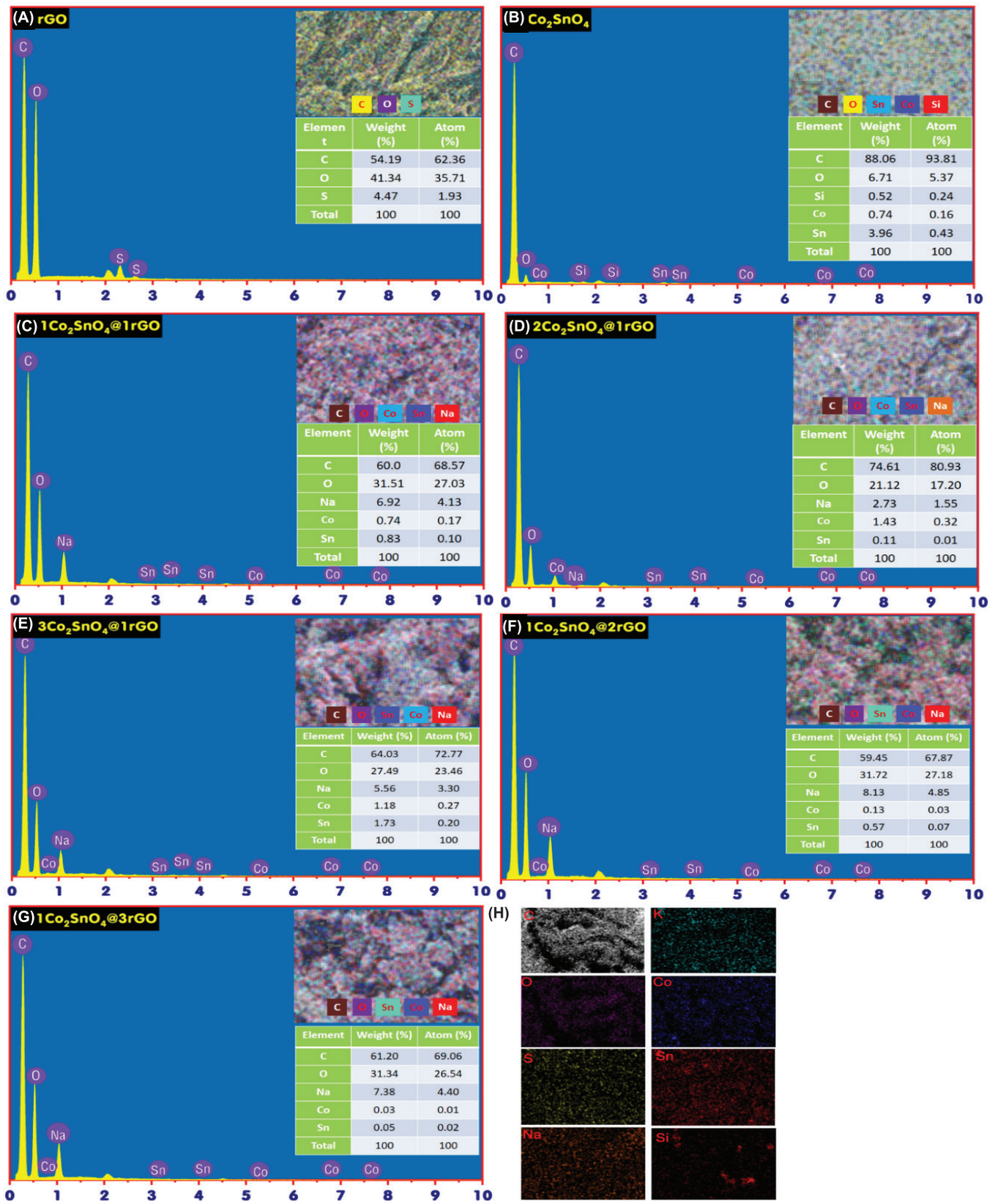

Fig. 4. EDX spectra of Co_2SnO_4@rGO at various modification ratios. (A) rGO, **(B)** Co_2SnO_4, **(C)** 1-Co_2SnO_4@1-rGO, **(D)** 2-Co_2SnO_4@1-rGO, **(E)** 3-Co_2SnO_4@1-rGO, **(F)** 1-Co_2SnO_4@2-rGO, **(G)** 1-Co_2SnO_4@3-rGO, **(H)** Mapping of Co_2SnO_4@rGO.

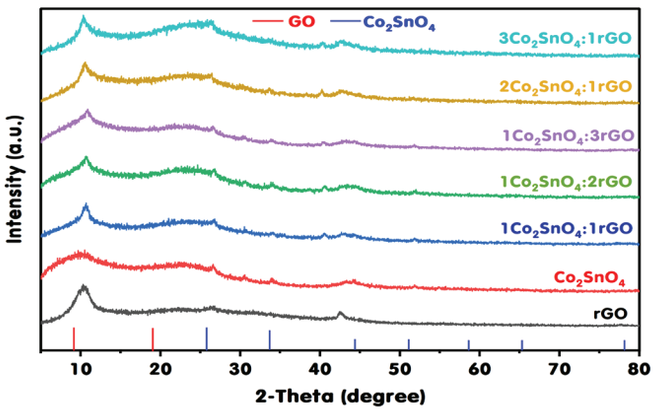

Fig. 5. XRD of catalysts at various modification ratios. (A) rGO, **(B)** Co_2SnO_4, **(C)** $1Co_2SnO_4$@1rGO, **(D)** $2Co_2SnO_4$@1rGO, **(E)** $3Co_2SnO_4$@1rGO, **(F)** $1Co_2SnO_4$@2rGO, **(G)** $1Co_2SnO_4$@3rGO.

successfully reduced to reduced graphene oxide [35] in the synthesis procedure. The observed diffraction peaks at 26.131, 34.321, 35.911, 44.711, 51.761, 57.111, 66.491 and 78.111° are indexed and well matched to cubic Co_2SnO_4 with the space group Fd3m (JCPDS No. 29-0514). The sharp intensity peaks denote the high crystallinity of Co_2SnO_4. It is worth noticing the presence of small diffraction peaks due to SnO_2 and $CoSn(OH)_6$.

The diffraction peaks of Co_2SnO_4@rGO at different composite ratios are consistent with that of Co_2SnO_4 indicating that Co_2SnO_4 was basically deposited on the surface of the graphene layer and its crystal form was unchanged during the synthesis. However, the characteristic peak of Co_2SnO_4@rGO at the ratio of 2-Co_2SnO_4:1-rGO is slightly wider and clearer in comparison with other ratios.

3.2. Catalytic performance of Co_2SnO_4@rGO in the Co_2SnO_4@rGO/PMS and O_3/Co_2SnO_4@rGO/PMS systems

To assess the catalytic activity of Co_2SnO_4@rGO at various composite ratios for PMS activation in Co_2SnO_4@rGO, Co_2SnO_4@rGO/PMS, and O_3/Co_2SnO_4@rGO/PMS systems, degradation experiments of CFX were conducted. The experiment to evaluate catalytic performance of the fabricated heterogeneous catalysts to activate PMS in the Co_2SnO_4@rGO/PMS and O_3/Co_2SnO_4@rGO/PMS systems were conducted with varying composite ratios of Co_2SnO_4:rGO, specifically, 1:1, 2:1: 3:1, 1:2, and 1:3 at an initial CFX concentration of 100 mg/l, PMS dosage of 300 mg/l, catalyst dosage of 0.3 g/l, and at a pH of 7. The results are presented in Fig. 6.

What stands out from the data in Figs. 6A, B is that the CFX degradation efficiencies were varied when the compositing ratios were changed. CFX degradation was completely achieved after 40 min of reaction time. The CFX degradation curves for both Co_2SnO_4@rGO/PMS and O_3/Co_2SnO_4@rGO/PMS systems followed the same trend.

The removal efficiency of CFX reached a peak at a composite ratio of 2-Co_2SnO_4 and 1-rGO in both system (95.07% for Co_2SnO_4@rGO/PMS and 99.07% for O_3/Co_2SnO_4@rGO/PMS).

The degradation of CFX was the lowest in both systems at a composite ratio of 1-Co_2SnO_4 and 1-rGO reaching 23.2 and 82.0%, respectively, for Co_2SnO_4@rGO/PMS and O_3 Co_2SnO_4@rGO/PMS. When increasing the amount of rGO, the degradation of CFX increased. The degradation efficiency of CFX in the O_3/Co_2SnO_4@rGO/PMS system was higher than that of Co_2SnO_4@rGO/PMS, showing a synergetic effect in the hybrid ozonation system for the removal of CFX from wastewater. The results showed that the composite ratio had a significant effect on CFX degradation efficiency in both treatment systems in this study.

Previous works have also suggested that the degradation of CFX by advanced $^{\bullet}SO_4^-$-based oxidation systems using heterogeneous catalysts for the activation of PMS follows a first-order model [28, 34]. Thus, in this work, the experimental degradation data of CFX at various composite ratios were fit with a first-order model and the obtained results are presented in Table 2. As expected, the R^2 values of the fit were very high. Besides, all k_d values agreed well with degradation results of CFX at various composite ratios between Co_2SnO_4 and rGO as discussed earlier. Among the composite ratios tested, 1-Co_2SnO_4 and 1-rGO was the most effective for degrading CFX. The k_d values were determined to be 0.007, 0.076, 0.033, 0.026, and 0.043 min^{-1} and 0.047, 0.112, 0.560, 0.047, 0.049 min^{-1} corresponded with composite ratios of $1Co_2SnO_4$@1rGO, $2Co_2SnO_4$@1rGO, $3Co_2SnO_4$@1rGO, $1Co_2SnO_4$@2rGO, and $1Co_2SnO_4$@3rGO for Co_2SnO_4@rGO/PMS and

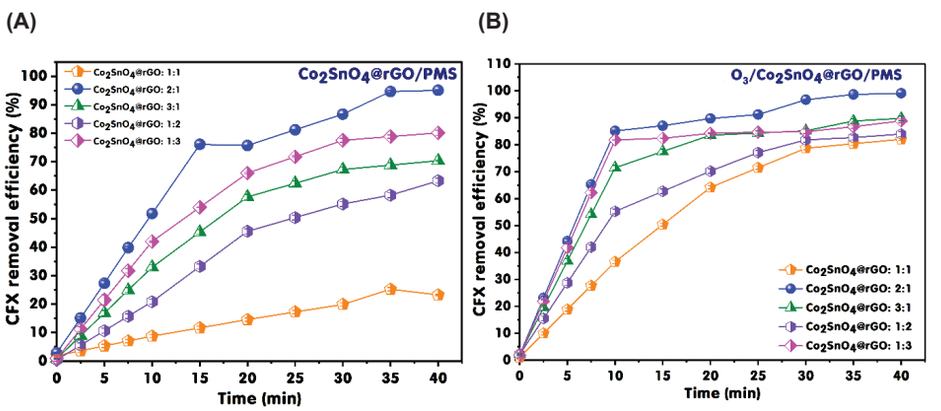

Fig. 6. Time evolution of CFX degradation by Co_2SnO_4@rGO/PMS (A) and O_3/Co_2SnO_4@rGO/PMS (B) at various modification ratios between Co_2SnO_4 and rGO.

Table 2. Degradation kinetic of CFX by Co_2SnO_4@rGO/PMS and O_3/Co_2SnO_4@rGO/PMS.

Reaction conditions		Co_2SnO_4@rGO/PMS		O_3/Co_2SnO_4@rGO/PMS	
		k_d (min^{-1})	R^2	k_d (min^{-1})	R^2
Modification (Co_2SnO_4@rGO)	1:1	0.007	0.9788	0.047	0.9852
	2:1	0.076	0.9736	0.112	0.9649
	3:1	0.033	0.9656	0.560	0.8984
	1:2	0.026	0.9882	0.047	0.9599
	1:3	0.043	0.9733	0.049	0.7308

O_3/Co_2SnO_4@rGO/PMS, respectively. The k_d value reached a peak at a composite ratio of 2-Co_2SnO_4 and 1-rGO for both reaction systems. The k_d values in the O_3/Co_2SnO_4@rGO/PMS system were higher than those in Co_2SnO_4@rGO/PMS at all composite ratios. The results showed that in the addition of O_3 into the Co_2SnO_4@rGO/PMS system promoted the degradation rate of CFX thanks to the synergetic effect of O_3 and Co_2SnO_4@rGO/PMS. Besides, the composition of rGO with Co_2SnO_4 nanoparticles remarkably increased the S_{BET} of the nanocomposite, specifically from 112.9 and 25.43 m^2/g, respectively, for rGO and Co_2SnO_4 to 435.432 m^2/g for 2-Co_2SnO_4@1-rGO. This result proved that the Co_2SnO_4 NPs were successfully loaded onto the surface of rGO. Such a high S_{BET} from the 2-Co_2SnO_4@1-rGO nanocomposite provided more adsorption/catalysis sites for activating PMS during the catalytic process, leading to higher catalytic activities for the degradation of CFX in both systems. Similar results were obtained by previous works. For example, D. Ge, et al. (2016) [36] indicated that the degradation of methyl orange in a O_3/Fe^{2+}/PS reactor increased because inlet ozone concentration enhanced the synergistic effect between ozone and persulphate, thus leading to a higher degradation rate of MO. O_3 was also proved to be enhancement of degradation rate of 4-nitrophenol in the O_3/MnO_2/rGO/PMS system thanks to the synergistic effect between catalytic ozonation and the coupling of PMS activation to generate more $^*SO_4^-$ and *OH radicals, leading to enhancement of pollutants degradation rate [14].

4. Conclusions

In this study, a heterogeneous catalyst derived from a composite of Co_2SnO_4 NPs and rGO at various composite ratios was successfully developed using the sol-gel method. The Co_2SnO_4NPs@rGO at different composite ratios were used to activate PMS in both Co_2SnO_4@rGO/PMS and O_3/Co_2SnO_4@rGO/PMS for the degradation of CFX. The degradation efficiencies of CFX in both systems followed the same trend. However, the removal efficiencies of CFX in hybrid ozonation were higher than those in Co_2SnO_4@rGO/PMS. The degradation of CFX was maximised at a composite ratio of 2-Co_2SnO_4 and 1-rGO. The material characteristics data showed that S_{BET} of the catalyst was remarkably improved at a composite ratio of 2-Co_2SnO_4 and 1-rGO, which facilitated more active sites on the catalyst to degrade CFX. Besides, the presence of Co in 2-Co_2SnO_4@1-rGO was the highest, leading to an enhancement of PMS activation to produce more $^*SO_4^-$. Notably, the combination of O_3 in the Co_2SnO_4@rGO/PMS reactor formed a synergetic effect to increase the generation of *OH radicals, leading to the promotion of CFX degradation rate to reach the standards of QCVN 40:2011/BTNMT (Column A).

CRediT author statement

Van Long Nguyen: Conceptualisation, Methodology, Software; Minh Thanh Le: Visualisation, Investigation, Data curation; Lan Huong Nguyen: Supervision, Writing - Original draft preparation, Writing - Reviewing and Editing.

ACKNOWLEDGEMENTS

The study was supported by Youth Incubator for Science and Technology Program, managed by Youth Development Science and Technology Center - Ho Chi Minh Communist Youth Union and Department of Science and Technology of Ho Chi Minh City under contract number 34/2021/HD-KHCNT-VU.

COMPETING INTERESTS

The authors declare that there is no conflict of interest regarding the publication of this article.

REFERENCES

[1] X.H. Wang, A.Y.C. Lin (2012), "Phototransformation of cephalosporin antibiotics in an aqueous environment results in higher toxicity", *Environ. Sci. Technol.*, **46(22)**, pp.12417-12426, DOI: 10.1021/es301929e.

[2] F. Tavasol, T. Tabatabaie, B. Ramavandi, et al. (2020), "Design a new photocatalyst of sea sediment/titanate to remove cephalexin antibiotic from aqueous media in the presence of sonication/ultraviolet/hydrogen peroxide: Pathway and mechanism for degradation", *Ultrason. Sonochem.*, **65(105062)**, DOI: 10.1016/j.ultsonch.2020.105062.

[3] K. Kümmerer (2009), "Antibiotics in the aquatic environment - A review - Part II", *Chemosphere*, **75(4)**, pp.435-441, DOI: 10.1016/j.chemosphere.2008.12.006.

[4] J. Chen, C. Fang, W. Xia, et al. (2018), "Selective transformation of β-lactam antibiotics by peroxymonosulfate: Reaction kinetics and nonradical mechanism", *Environ. Sci. Technol.*, **52(3)**, pp.1461-1470, DOI: 10.1021/acs.est.7b05543.

[5] Y. Qian, G. Xue, J. Chen, et al. (2018), "Oxidation of cefalexin by thermally activated persulfate: Kinetics, products, and antibacterial activity change", *J. Hazard. Mater.*, **354,** pp.153-160, DOI: 10.1016/j.jhazmat.2018.05.004.

[6] C. Su, X. Lin, P. Zheng, et al. (2019), "Effect of cephalexin after heterogeneous Fenton-like pretreatment on the performance of anaerobic granular sludge and activated sludge", *Chemosphere*, **235**, pp.84-95, DOI: 10.1016/j.chemosphere.2019.06.136.

[7] P. Bansal, A. Verma, C. Mehta, et al. (2018), "Assessment of integrated binary process by coupling photocatalysis and photo-Fenton for the removal of cephalexin from aqueous solution", *J. Mater. Sci.*, **53(10)**, pp.7326-7343, DOI: 10.1007/s10853-018-2094-x.

[8] R. Mirzaei, M. Yunesian, S. Nasseri, et al. (2018), "Occurrence and fate of most prescribed antibiotics in different water environments of Tehran, Iran", *Sci. Total Environ.*, **619-620**, pp.446-459, DOI: 10.1016/j.scitotenv.2017.07.272.

[9] S. Li, W. Shi, W. Liu, et al. (2018), "A duodecennial national synthesis of antibiotics in China's major rivers and seas (2005-2016)", *Sci. Total Environ.*, **615**, pp.906-917, DOI: 10.1016/j.scitotenv.2017.09.328.

[10] T.B. Minh, H.W. Leung, I.H. Loi, et al. (2009), "Antibiotics in the Hong Kong metropolitan area: Ubiquitous distribution and fate in Victoria Harbour", *Mar. Pollut. Bull.*, **58(7)**, pp.1052-1062, DOI: 10.1016/j.marpolbul.2009.02.004.

[11] S.G. Cordeiro, R. Ziem, Y.A. Schweizer, et al. (2021), "Degradation of micropollutant cephalexin by ultraviolet (UV) and assessment of residual antimicrobial activity of transformation products", *Water Sci. Technol.*, **84(2)**, pp.374-383, DOI: 10.2166/wst.2021.170.

[12] R. Guo, J. Chen (2015), "Application of alga-activated sludge combined system (AASCS) as a novel treatment to remove cephalosporins", *Chem. Eng. J.*, **260**, pp.550-556, DOI: 10.1016/j.cej.2014.09.053.

[13] Z. Yuan, M. Sui, B. Yuan, et al. (2017), "Degradation of ibuprofen using ozone combined with peroxymonosulfate", *Environ. Sci. Water Res. Technol.*, **3(5)**, pp.960-969, DOI: 10.1039/C7EW00174F.

[14] Y. Wang, Y. Xie, H. Sun, et al. (2016), "2D/2D nano-hybrids of γ-MnO_2 on reduced graphene oxide for catalytic ozonation and coupling peroxymonosulfate activation", *J. Hazard. Mater.*, **301**, pp.56-64, DOI: 10.1016/j.jhazmat.2015.08.031.

[15] J. Cong, G. Wen, T. Huang, et al. (2015), "Study on enhanced ozonation degradation of para-chlorobenzoic acid by peroxymonosulfate in aqueous solution", *Chem. Eng. J.*, **264**, pp.399-403, DOI: 10.1016/j.cej.2014.11.086.

[16] F. Chi, G. Zhou, B. Song, et al. (2016), "$CoTiO_3$ nanoparticles as a highly active heterogeneous catalyst of peroxymonosulfate for the degradation of organic pollutants under visible-light illumination", *J. Nano Res.*, **42**, pp.73-79, DOI: 10.4028/www.scientific.net/jnanor.42.73.

[17] M. Stoyanova, I. Slavova, S. Christoskova, et al. (2014), "Catalytic performance of supported nanosized cobalt and iron-cobalt mixed oxides on MgO in oxidative degradation of acid orange 7 azo dye with peroxymonosulfate", *Appl. Catal. A Gen.*, **476**, pp.121-132, DOI: 10.1016/j.apcata.2014.02.024.

[18] Y. Ren, L. Lin, J. Ma, et al. (2015), "Sulfate radicals induced from peroxymonosulfate by magnetic ferrospinel MFe_2O_4 (M=Co, Cu, Mn, and Zn) as heterogeneous catalysts in the water", *Applied Catalysis B: Environmental*, **165**, pp.572-578, DOI: 10.1016/j.apcatb.2014.10.051.

[19] Y. Yao, Y. Cai, G. Wu, et al. (2015), "Sulfate radicals induced from peroxymonosulfate by cobalt manganese oxides (Co_xMn_3-xO_4) for Fenton-Like reaction in water", *J. Hazard. Mater.*, **296**, pp.128-137, DOI: 10.1016/j.jhazmat.2015.04.014.

[20] X. Li, Z. Wang, B. Zhang, et al. (2016), "Fe_xCo_3-xO_4 nanocages derived from nanoscale metal-organic frameworks for removal of bisphenol A by activation of peroxymonosulfate", *Applied Catalysis B: Environmental*, **181**, pp.788-799, DOI: 10.1016/j.apcatb.2015.08.050.

[21] H. Bouchaaba, B. Bellal, R. Maachi, et al. (2016), "Optimization of physico-chemical parameters for the photo-oxidation of neutral red on the spinel Co_2SnO_4", *J. Taiwan Inst. Chem. Eng.*, **58**, pp.310-317, DOI: 10.1016/j.jtice.2015.06.011.

[22] M. Golshan, B. Kakavandi, M. Ahmadi, et al. (2018), "Photocatalytic activation of peroxymonosulfate by TiO_2 anchored on cupper ferrite (TiO_2@$CuFe_2O_4$) into 2,4-D degradation: Process feasibility, mechanism and pathway", *J. Hazard. Mater.*, **359**, pp.325-337, DOI: 10.1016/j.jhazmat.2018.06.069.

[23] Q. Yang, H. Choi, Y. Chen, et al. (2008), "Heterogeneous activation of peroxymonosulfate by supported cobalt catalysts for the degradation of 2,4-dichlorophenol in water: The effect of support, cobalt precursor, and UV radiation", *Applied Catalysis B: Environmental*, **77(3-4)**, pp.300-307, DOI: 10.1016/j.apcatb.2007.07.020.

[24] Y. Wang, H. Sun, H.M. Ang, et al. (2014), "Magnetic Fe_3O_4/carbon sphere/cobalt composites for catalytic oxidation of phenol solutions with sulfate radicals", *Chem. Eng. J.*, **245**, pp.1-9, DOI: 10.1016/j.cej.2014.02.013.

[25] P.R. Shukla, S. Wang, H. Sun, et al. (2010), "Activated carbon supported cobalt catalysts for advanced oxidation of organic contaminants in aqueous solution", *Applied Catalysis B: Environmental*, **100(3-4)**, pp.529-534, DOI: 10.1016/j.apcatb.2010.09.006.

[26] Z. Huang, H. Bao, Y. Yao, et al. (2016), "Key role of activated carbon fibers in enhanced decomposition of pollutants using heterogeneous cobalt/peroxymonosulfate system", *J. Chem. Technol. Biotechnol.*, **91(5)**, pp.1257-1265, DOI: 10.1002/jctb.4715.

[27] A.H. Mady, M.L. Baynosa, D. Tuma, et al. (2019), "Heterogeneous activation of peroxymonosulfate by a novel magnetic 3D Γ-MnO_2@$ZnFe_2O_4$/rGO nanohybrid as a robust catalyst for phenol degradation", *Applied Catalysis B: Environmental*, **244**, pp.946-956, DOI: 10.1016/j.apcatb.2018.11.086.

[28] E.B. Lashkaryani, B. Kakavandi, R.R. Kalantary, et al. (2019), "Activation of peroxymonosulfate into amoxicillin degradation using cobalt ferrite nanoparticles anchored on graphene ($CoFe_2O_4$@Gr)", *Toxin Rev.*, **40(2)**, pp.215-224, DOI: 10.1080/15569543.2019.1582066.

[29] N. Mengelizadeh, E. Mohseni, M.H. Dehghani (2021), "Heterogeneous activation of peroxymonosulfate by GO-$CoFe_2O_4$ for degradation of reactive black 5 from aqueous solutions: Optimization, mechanism, degradation intermediates and toxicity", *J. Mol. Liq.*, **327**, DOI: 10.1016/j.molliq.2020.114838.

[30] R. Tabit, O. Amadine, Y. Essamlali, et al. (2018), "Magnetic $CoFe_2O_4$ nanoparticles supported on graphene oxide ($CoFe_2O_4$/GO) with high catalytic activity for peroxymonosulfate activation and degradation of rhodamine B", *RSC Adv.*, **8(3)**, pp.1351-1360, DOI: 10.1039/C7RA09949E.

[31] Y. Yao, Z. Yang, D. Zhang, et al. (2012), "Magnetic $CoFe_2O_4$-graphene hybrids", *Ind. Eng. Chem. Res.*, **17**, pp.6044-6051, DOI: 10.1021/ie300271p.

[32] L. Zou, X. Xiao, C. Chu, et al. (2021), "Facile synthesis of porous $CoFe_2O_4$/graphene aerogel for catalyzing efficient removal of organic pollutants", *Sci. Total Environ.*, **775**, DOI: 10.1016/j.scitotenv.2020.143398.

[33] W.S. Hummers, R.E. Offeman (1958), "Preparation of graphitic oxide", *J. Am. Chem. Soc.*, **80(6)**, DOI: 10.1021/ja01539a017.

[34] M.B. Ali, A. Barras, A. Addad, et al. (2017), "Co_2SnO_4 nanoparticles as a high performance catalyst for oxidative degradation of rhodamine B dye and pentachlorophenol by activation of peroxymonosulfate", *Phys. Chem. Chem. Phys.*, **19(9)**, pp.6569-6578, DOI: 10.1039/C6CP08576H.

[35] Y. Zhao, G. Nie, X. Ma, et al. (2019), "Peroxymonosulfate catalyzed by rGO assisted $CoFe_2O_4$ catalyst for removing Hg0 from flue gas in heterogeneous system", *Environ. Pollut.*, **249**, pp.868-877, DOI: 10.1016/j.envpol.2019.03.103.

[36] D. Ge, Z. Zeng, M. Arowo, et al. (2016), "Degradation of methyl orange by ozone in the presence of ferrous and persulfate ions in a rotating packed bed", *Chemosphere*, **146**, pp.413-418, DOI: 10.1016/j.chemosphere.2015.12.058.